2020 American Control Conference
Denver, CO, USA, July 1-3, 2020

A Task-Invariant Learning Framework of Lower-Limb Exoskeletons for Assisting Human Locomotion

Ge Lv*, Haosen Xing*, Jianping Lin, Robert D. Gregg, Christopher G. Atkeson

Abstract— **Kinematic control approaches for exoskeletons follow specified trajectories, which overly constrain individuals who have partial or full volitional control over their lower limbs. In our prior work, we proposed a general matching framework for underactuated energy shaping to provide task-invariant, energetic exoskeletal assistance. While the proposed shaping strategies demonstrated benefits such as reduced human torques during walking, it remains unclear how the parameters of these shaping strategies are related to different gait benefits. Meanwhile, research indicates that customizing assistance via online optimization can substantially improve exoskeleton's performance for each individual. Motivated by this fact, we combine derivative-free, sample-efficient optimization algorithms with our energy shaping strategies to propose a task-invariant learning framework for lower-limb exoskeletons. Through rapid online optimization, this framework enables exoskeletons to adjust shaping parameters for minimizing human joint torques across users and tasks. Simulation results show that shaping strategies with optimal parameters effectively reduce human joint torques and estimated metabolic cost during simulated walking. In addition, the optimal exoskeleton torques calculated using able-bodied subjects' kinematic data closely match the real human joint torques for different walking gaits.**

I. INTRODUCTION

The majority of powered lower-limb exoskeletons adopt kinematic control methods to replicate normative joint kinematics [1]–[4]. These devices follow trajectories associated with one specific task and user at a time [5], which do not translate well across continuously varying locomotor tasks or changes in user behavior. While this may be useful for individuals who cannot volitionally control their lower limbs, individuals with at least some volitional control ability should be allowed to choose their preferred gait patterns or make corrections during gait therapy. Moreover, in order to accurately track different reference trajectories, task recognition is often required in practice, which is currently difficult to achieve [6]. A paradigm shift from task-specific, kinematic control approaches to task-invariant approaches is needed for exoskeleton control design.

Instead of enforcing kinematic trajectories, we can enforce energetic goals to provide exoskeletal assistance with greater freedom and flexibility. As a kinetic control method, energy shaping has been applied to bipedal locomotion to create natural, efficient gaits based on passive dynamics [7], regulate a biped's walking speed [8], and facilitate 3D walking gaits via control reduction [9]. In our prior work [10], we proposed an energetic control approach that shapes the potential and kinetic energies of the human body through the actuators of an exoskeleton in the closed loop. By shaping potential energy, torques can be generated to counteract gravity to yield the so-called body-weight support (BWS), which offloads the perceived weight of the user's lower extremities and center of mass (COM). By shaping kinetic energy, we can assist the subject's acceleration/deceleration by compensating inertial terms along the diagonal [11] or in all entries [10] in the bottom-right part of a mass matrix. Simulation results on total energy shaping [12] and experimental results on potential energy shaping [10], [13] have demonstrated potential beneficial results in assisting different gaits.

Despite these promising results, it remains unclear how the choices of energy shaping parameters are related to different gait benefits. The shaping parameters in prior work, i.e., the BWS ratio and the inertia scaling factors, were chosen arbitrarily based on intuitions. In stroke gait rehabilitation, the BWS ratio is usually chosen by clinicians based on empirical data [14]. As the subjects make progress through training, the clinicians will gradually lower the BWS percentage to provide less support and allow more independence. While this is apparent for gait rehabilitation, choosing parameters for gait augmentation is not straightforward. For gait augmentation, a key metric for evaluating an exoskeleton is whether it reduces the human user's metabolic cost of walking [15]. Prior work [16], [17] showed that rapid, customized assistive strategies obtained via human-in-the-loop optimization led to substantial metabolic reduction during walking. However, these approaches only focus on optimizing exoskeleton torque for one joint during certain phases of a gait cycle. Generalizing these results to simultaneously optimize control parameters for multiple actuators throughout the entire gait cycle can possibly yield more benefits for gait augmentation.

To address these issues, we present a task-invariant learning framework for lower-limb exoskeletons to optimize exoskeleton actuator torques during various activities. Instead of optimizing parameters for a single joint's kinematic trajectory, we optimize parameters of the previously proposed energy shaping strategies for multiple human joints. To formulate the framework, we choose the Covariance Matrix Adaptation Evolution Strategy (CMA-ES) [18] and Bayesian Optimization (BO) [19] given their prevalence in bipedal locomotion related research [16], [20]. We use the integral

* *indicates both authors contributed equally to this work.*

G. Lv is with the Department of Mechanical Engineering, Clemson University, Clemson, SC 29634. H. Xing, and C. Atkeson are with the Robotics Institute, Carnegie Mellon University, Pittsburgh, PA 15213. J. Lin and R. Gregg are with the Robotics Institute, University of Michigan, Ann Arbor, MI 48109. glv@clemson.edu

This work is supported by NSF Awards 1734449, 1652514, and 1949869. R. D. Gregg holds a Career Award at the Scientific Interface from the Burroughs Wellcome Fund. The content is solely the responsibility of the authors and does not necessarily represent the official view of the NSF.

of squared human joint torques proposed in [21] as our cost function, where the human torque is calculated through the Euler-Lagrange dynamics. By minimizing this cost function, we minimize the correlated muscle activation, which in turn is believed to be correlated with metabolic cost [22]. Because of the task-invariant property of our energy shaping strategies, the proposed framework enables an exoskeleton to automatically select optimal control parameters to assist individuals with various activities.

The rest of the paper is organized as follows: we begin in Section II by reviewing the human-exoskeleton dynamics and prior results on energy shaping. In Section III, we introduce CMA-ES and BO to formulate the task-invariant learning framework. Finally, we show benefits for gait augmentation with simulations on an 8-degree of freedom (DOF) biped and the exoskeleton torques computed based on able-bodied subjects' kinematic data in Section IV.

II. Dynamics and Energy Shaping

A. Human and Exoskeleton Model

We first review the sagittal biped model and its dynamics presented in [10]. For simplicity, we combine the biped's two hip joints into one and assume the biped's mass consists of the mass of exoskeleton links and human legs. The planar biped shown in Fig. 1 is modeled as a kinematic chain with respect to an inertial reference frame (IRF). Depending on whether the exoskeleton is unilateral or bilateral, we choose to model the stance and swing legs separately (unilateral case [12]) or the entire lower body as a kinematic chain from the stance foot to the swing foot (bilateral case [11]). By explicitly modeling contact constraints in the dynamics, the equations of motion can be expressed as

$$M\ddot{q} + C\dot{q} + N + A^T\lambda = \tau, \tag{1}$$

where $M \in \mathbb{R}^{n\times n}$ is the positive-definite mass matrix with n being the number of DOFs, $C \in \mathbb{R}^{n\times n}$ is the Coriolis/centrifugal matrix, and $N \in \mathbb{R}^n$ is the gravitational forces vector. The configuration space is given as $\mathcal{Q} = \mathbb{R}^2 \times \mathbb{T}^{(n-2)}$, and the corresponding configuration vector is $q = (\theta_{\mathrm{x}}, \theta_{\mathrm{y}}, \theta_{\mathrm{ab}}, q_{\mathrm{s}}^T)^T \in \mathbb{R}^n$, where $\mathbb{T}^{(n-2)}$ is the $(n-2)$ torus, θ_{x} and θ_{y} are the Cartesian coordinates with respect to the IRF, and $\theta_{\mathrm{ab}} \in \mathbb{S}^1$ is an absolute angle defined with respect to the vertical axis. The shape vector $q_{\mathrm{s}} \in \mathbb{R}^{n-3}$ contains joint angles based on the biped model. The matrix $A^T \in \mathbb{R}^{n\times c}$ is the constraint matrix defined as the gradient of the holonomic constraint functions, and c is the number of contact constraints that change during different contact conditions. The Lagrange multiplier λ is calculated using the method in [23] as

$$\lambda = \hat{\lambda} + \bar{\lambda}\tau, \tag{2}$$

where

$$\begin{aligned} \hat{\lambda} &= W[\dot{A}\dot{q} - AM^{-1}(C\dot{q} + N)], \\ \bar{\lambda} &= WAM^{-1}, \;\; W = (AM^{-1}A^T)^{-1}. \end{aligned} \tag{3}$$

Because we are modeling the human body and the exoskeleton as a whole, the torque $\tau = \tau_{\mathrm{hum}} + \tau_{\mathrm{exo}}$ at the right-hand side of (1) comprises both the human and the exoskeleton input terms, $\tau_{\mathrm{hum}} = Bv + J^TF$ and $\tau_{\mathrm{exo}} = Bu$, respectively. The mapping matrix $B \in \mathbb{R}^{n\times p}$ maps both the human muscle input term $v \in \mathbb{R}^p$ and the exoskeleton actuator torques $u \in \mathbb{R}^p$ into the dynamics. Without loss of generality, we assume B takes the form of $[0_{p\times(n-p)}, \;\; I_{p\times p}]^T$. In general, the vector F includes the interaction forces between the modeled subsystem and the connected un-modeled links. For unilateral models, the body *Jacobian* matrix $J^T \in \mathbb{R}^{n\times 3}$ maps the interaction forces $F = (F_{\mathrm{x}}, F_{\mathrm{y}}, M_z)^T \in \mathbb{R}^3$ in τ_{hum} into the dynamics, where $(F_{\mathrm{x}}, F_{\mathrm{y}})^T$ indicates two linear forces, and M_{z} indicates a moment in the sagittal plane. For bilateral cases, we combine stance and swing leg models and implicitly model F in the equations of motions of the kinematic chain.

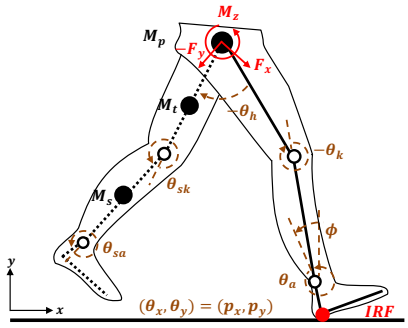

Fig. 1. Kinematic model of the human body and the exoskeleton(s). The stance leg is shown in solid black and the swing leg in dashed black. The IRF is defined at the heel (shown here), and $(\theta_{\mathrm{x}}, \theta_{\mathrm{y}})$ is chosen as the heel position $(p_{\mathrm{x}}, p_{\mathrm{y}})$ for the model used in simulation.

B. Holonomic Contact Constraints

The single-support period of human walking can be separated into heel contact, flat foot, and toe contact phases, as shown in [10, Figure 11]. The general form of holonomic contact constraints encountered during these conditions can be expressed as relations between the position variables, i.e.,

$$a(q_1, q_2, ..., q_c) = 0_{c\times 1}, \tag{4}$$

where q_i denotes the i-th element of the configuration vector q. Based on different contact conditions, there are $c = 2$ constraints for heel contact and toe contact, whereas flat foot has $c = 3$. In this paper, we assume the constraint matrix A has the constant form

$$A = \nabla_q a(q_1, q_2, ..., q_c) = [I_{c\times c} \quad 0_{c\times(n-c)}]. \tag{5}$$

The constant form (5) (i.e., $\dot{A} = 0$) can be achieved by defining the IRF at the stance toe during toe contact and at the stance heel during heel and flat foot contact. Note that for a unilateral model's swing leg, there are no contact constraints defined, i.e., $A = 0$.

C. Shapeable Dynamics

In this section, we review the equivalent constrained dynamics (ECD) and our prior results on the shapeable

dynamics of ECD. We omit the detailed matching proof and refer the readers to [10].

By plugging the expressions for A and λ into (1), we can obtain the ECD of (1) as

$$M_\lambda \ddot{q} + C_\lambda \dot{q} + N_\lambda = B_\lambda v + J_\lambda^T F + B_\lambda u, \tag{6}$$

where

$$\begin{aligned} M_\lambda &= M, \\ C_\lambda &= (I - A^T W A M^{-1}) C, \\ N_\lambda &= (I - A^T W A M^{-1}) N, \\ B_\lambda &= (I - A^T W A M^{-1}) B, \\ J_\lambda^T &= (I - A^T W A M^{-1}) J^T. \end{aligned} \tag{7}$$

Dynamics in the form of (6) has fewer or zero unactuated DOFs compared to the generalized dynamics (1) without constraints. Given the open-loop dynamics (6), we define the desired closed-loop ECD as

$$\tilde{M}_\lambda \ddot{q} + \tilde{C}_\lambda \dot{q} + \tilde{N}_\lambda = \tilde{B}_\lambda v + \tilde{J}_\lambda^T F, \tag{8}$$

where $\tilde{M}_\lambda = \tilde{M}$ is the mass matrix in the closed-loop ECD and is assumed to be positive-definite. The remaining terms in (8) are given by

$$\begin{aligned} \tilde{C}_\lambda &= (I - A^T \tilde{W} A \tilde{M}^{-1}) \tilde{C}, \\ \tilde{N}_\lambda &= (I - A^T \tilde{W} A \tilde{M}^{-1}) \tilde{N}, \\ \tilde{B}_\lambda &= (I - A^T \tilde{W} A \tilde{M}^{-1}) \tilde{B}, \\ \tilde{J}_\lambda^T &= (I - A^T \tilde{W} A \tilde{M}^{-1}) \tilde{J}^T, \\ \tilde{W} &= (A \tilde{M}^{-1} A^T)^{-1}, \end{aligned} \tag{9}$$

with $\tilde{C}$ and $\tilde{N}$ being the dynamics terms of (1) in closed loop. The detailed choices of these closed-loop dynamics terms will be specified later in the simulation section.

Our prior work [10] shows that the matching condition for mechanical energy is satisfied with the following choice of closed-loop dynamics

$$\tilde{M} = \begin{bmatrix} M_1 & M_2 \\ M_2^T & \tilde{M}_4 \end{bmatrix}, \quad \tilde{N} = \begin{bmatrix} N_{(1,n-p)} \\ \tilde{N}_{(n-p+1,n)} \end{bmatrix},$$

where $M_1 \in \mathbb{R}^{(n-p)\times(n-p)}$, $M_2 \in \mathbb{R}^{(n-p)\times p}$, $M_4 \in \mathbb{R}^{p\times p}$. By shaping these dynamics, the matching condition for the human input term will be automatically satisfied. The control law that brings (6) into (8) becomes

$$u = B_\lambda^+ [C_\lambda \dot{q} + N_\lambda - M_\lambda \tilde{M}_\lambda^{-1} (\tilde{C}_\lambda \dot{q} + \tilde{N}_\lambda)], \tag{10}$$

where $B_\lambda^+ = (B_\lambda^T B_\lambda)^{-1} B_\lambda^T$ is the left pseudo inverse of B_λ.

III. Learning Framework Formulation

In this section, we first review the algorithms of CMA-ES and BO. We then incorporate them with the previously proposed energy shaping to propose a task-invariant learning framework.

A. Covariance Matrix Adaptation Evolutionary Strategy

CMA-ES is a sample-efficient method for real-parameter optimization of nonlinear, non-convex function [18]. This optimization strategy comprises both measurement noise during real-time experiments and human adaptation [16], which makes it an ideal candidate for our approach. The detailed algorithm is shown in Algorithm 1, where definitions for hyper-parameters are shown in Table I.

The basic two perspectives of this algorithm, recombination and mutation, can be interpreted as selecting a new mean value $\mathbf{m}^{(i+1)}$ for the distribution and adding a random vector $\mathbf{z}_k^{i+1}$. The next generation mean value $\mathbf{m}^{(i+1)}$ represents the best estimation of optimal control parameters obtained after current population, and new candidate solutions are sampled according to a multivariate normal distribution $\mathcal{N}(0, \mathbf{I}) \in \mathbb{R}^n$. The terms $\mathbf{C}$, σ, $\mathbf{p}_\sigma$, and $\mathbf{p_c}$ are updated following the standard procedure in [18], and ω_j is chosen based on empirical data.

Algorithm 1 CMA-ES

Initialize $\mathbf{X}$ ▷ shaping parameters
Initialize $[q, \dot{q}]$ ▷ conditions for simulation
Initialize $\mathbf{m}^{(0)}, \sigma^{(0)}, \mathbf{C}^{(0)}, \mathbf{p}_\sigma{}^{(0)}, \mathbf{p_c}{}^{(0)}$ ▷ CMA-ES parameters
for $i = 0$ to Iter **do**
  for $k = 1$ to χ **do** ▷ sample new population
    $\mathbf{z}_k^{(i+1)} \sim \mathcal{N}(0, \mathbf{I})$
    $\mathbf{X}_k^{(i+1)} = \mathbf{m}^{(i)} + \sigma^{(i)} \mathbf{B}\mathbf{D}\mathbf{z}_k^{(i+1)}$ ▷ sample candidate solution
    simulate walking until convergence
    if stability guaranteed **then**
      $i = i + 1$, compute cost function
    end if
  end for
  $\mathbf{m}^{(i+1)} = \sum_{j=1}^{\gamma} w_j \mathbf{X}_{j\in[1,\ \chi]}^{(i+1)}$ ▷ sort the best γ candidates
  if gait stable with $\mathbf{m}^{(i+1)}$ **then**
    update $[q, \dot{q}]$, $\mathbf{C}^{(i+1)}$, $\sigma^{(i+1)}$, $\mathbf{p}_\sigma{}^{(i+1)}$, $\mathbf{p_c}{}^{(i+1)}$
  else
    $i = i - \chi$
  end if
end for

B. Bayesian Optimization

BO is a noise-tolerant and sample-efficient global optimization method, which selects new parameters using non-parametric regression models and principled metrics [24]. BO consists of two main components: a Bayesian statistical model for modeling the objective function, and an acquisition function for deciding where to sample next [25]. After evaluating the objective function based on some initial conditions, BO optimizes the acquisition function to select the next sample point.

The whole algorithm is shown in Algorithm 2. Similar to CMA-ES, the input $\mathbf{X}$ is the set of energy shaping strategy

TABLE I
PARAMETERS OF CMA-ES

Parameter	Definition
χ	Population size
Iter	Total iteration number
$\mathbf{X}$	Control parameters set
γ	Number of shaping parameters
$\mathbf{m}^{(i)}$	Mean value of the i-th iteration
$\sigma^{(i)}$	Step size of the i-th iteration
$\mathbf{C}^{(i)}$	Covariance matrix of the i-th iteration
$\mathbf{B}, \mathbf{D}$	Orthogonal and diagonal matrices
ω_j	Weight of $\mathbf{X}_j$, $\sum_{j=1}^{\gamma} \omega_j = 1$
$\mathbf{p}_\sigma$	Evolutionary path for σ
$\mathbf{p}_c$	Evolutionary path for $\mathbf{C}$

parameters, Iter is the total iteration number. The cost function is denoted as f, and data set D composes of different sets of previously generated $\mathbf{X}$. As in standard literature [24], $P(f)$ is a Gaussian process prior, $P(f|D)$ is the distribution posterior, and $C(\mathbf{X}|P(f|D))$ is the acquisition function. The state $[q, \dot{q}]$ will be updated corresponding to the change of $\mathbf{X}$ only if the generated gait is stable and the value of cost function is lower than previous iterations.

Algorithm 2 Bayesian Optimization

Initialize $\mathbf{X}$ ▷ shaping parameters
Initialize $[q, \dot{q}]$ ▷ conditions for simulation
$f(\mathbf{X})$ ▷ objective function
BAYESOPT(f, $\mathbf{X}$, Iter) ▷ Bayesian optimization
function $y = f(\mathbf{X})$
    simulate walking until convergence in $[q, \dot{q}]$
    if stability guaranteed **then**
        compute cost function
    end if
end function
function BAYESOPT(f, $\mathbf{X}$, Iter)
    $f_{\min} = f(\mathbf{X})$
    for $n = 1$ to Iter **do**
        $P(f|D) = \int P(D|f,\theta)P(f)P(\theta)\mathrm{d}\theta$ ▷ Bayes rule
        $\mathbf{X}_n = \text{argmax } C(\mathbf{X}|P(f|D))$
        Call $y_n = f(\mathbf{X}_n)$
        if $y_n < f_{\min}$ **then**
            $f_{\min} = y_n$
        end if
        $D = D \cup \{\mathbf{X}_n, y_n\}$ ▷ augment data
        if $y_n = f_{\min}$ **and** gait stable **then**
            update $[q, \dot{q}]$
        end if
        $n = n + 1$
    end for
end function

C. Optimization Formulation

Prior research [22] indicates that muscle activation squared is correlated with metabolic cost. By assuming that human joint torque squared is correlated to muscle activation squared, authors of [21] proposed a simulation-based metric for metabolic cost as

$$\sum_{j=1}^{p} \alpha_j^2 = \frac{\int_0^T \tau_{\text{hum}}^2(t)\mathrm{d}t}{T(mgl)^2} \approx \frac{\sum_{i=1}^{N_T} \tau_{\text{hum}}^2(i)\Delta t(i)}{T(mgl)^2}, \quad (11)$$

where T is the step time period, N_T is the number of timesteps in the simulation, $\Delta t(i)$ is the i-th timestep, m is the overall mass of the biped, and l is the length of the leg. We divide the human torque squared by $T(mgl)^2$ in (11) to isolate the effects of changing gait characteristics so that human joint torque squared can be compared across different shaping strategies. Finally, our optimization problem can be formulated as:

$$\begin{aligned} \underset{\mathbf{X}}{\text{minimize}} \quad & \sum_{j=1}^{p} \alpha_j^2 \approx \frac{\sum_{i=1}^{N_T} \tau_{\text{hum}}^2(i)\Delta t(i)}{T(mgl)^2} \\ \text{subject to} \quad & \tau_{\text{hum}} = \tilde{M}_\lambda \ddot{q} + \tilde{C}_\lambda \dot{q} + \tilde{N}_\lambda, \\ & \text{eig}(\tilde{M}_\lambda) > 0, \mathbf{X} \subset \bar{\mathbf{X}}, \\ & |\tau_{\text{exo}}| < \text{sat}, \\ & \text{Stability checked by Poincaré section method} \end{aligned}$$

where "sat" is the saturation for exoskeleton torques, and $\bar{\mathbf{X}}$ is the set of parameter ranges (will be specified later for different shaping strategies). Based on prior results [10], reducing mass and/or inertial parameters in the shapeable part of the inertia matrix can possibly reduce metabolic cost during simulated walking. However, reducing inertial and mass parameters arbitrarily in $\tilde{M}_4$ cannot ensure the positive definiteness of $\tilde{M}_\lambda$. We therefore include $\text{eig}(\tilde{M}_\lambda) > 0$ as a constraint in the formulation to avoid non-positive definite inertia matrix in the closed loop.

Note that the Poincaré section method is only used in simulation to ensure gait stability. In practice, we can establish a passive relationship from human input to joint velocity similar to [12] to ensure safe human-robot interaction. Also, estimating human joint torque in the cost function depends on the available sensors of an exoskeleton, e.g., IMU sensors and encoders for measuring joint kinematics.

IV. SIMULATION RESULTS AND DISCUSSION

To simulate human-like walking gaits, we consider the coupled dynamics of the two legs shown in Fig. 1, which is termed as the full biped model and is modeled as a kinematic chain with respect to the IRF defined at the stance heel. The configuration vector of the full biped model is given as $\theta = (\theta_{\text{x}}, \theta_{\text{y}}, \theta_{\text{ab}}, q_s^T)^T = (p_{\text{x}}, p_{\text{y}}, \phi, \theta_{\text{a}}, \theta_{\text{k}}, \theta_{\text{h}}, \theta_{\text{sk}}, \theta_{\text{sa}})^T \in \mathbb{R}^8$, where $(\theta_{\text{x}}, \theta_{\text{y}})^T = (p_{\text{x}}, p_{\text{y}})^T$ are the Cartesian coordinates of the stance heel, $\theta_{\text{ab}} = \phi$ is the stance heel angle defined with respect to the vertical axis. The shape vector is defined as $q_s = (\theta_{\text{a}}, \theta_{\text{k}}, \theta_{\text{h}}, \theta_{\text{sk}}, \theta_{\text{sa}})^T$, θ_{a} and θ_{sa} are angles of the stance and swing ankle, θ_{k} and θ_{sk} are angles of the stance and swing knee, and θ_{h} is the hip angle between the stance and swing thighs. The model and simulation parameters were adopted from [10, Table I].

A. Hybrid Dynamics and Stability

Biped locomotion can be modeled as a hybrid dynamical system that includes continuous and discrete dynamics. For the biped model we used in this paper, impacts happen when the swing heel contacts the ground and when contact constraints change between the heel contact and flat foot conditions. The following sequence that includes hybrid dynamics and impact maps during one step is a review of Section V-B in [12]:

1. $\mathcal{M}\ddot{\theta} + \mathcal{N} + \mathcal{A}_{\text{heel}}^T \lambda = \tau_{\text{e}} + \tau_{\text{h}}$ if $a_{\text{flat}} \neq 0$,
2. $\dot{\theta}^+ = (I - \mathcal{W}(\mathcal{A}_{\text{flat}}\mathcal{W})^{-1}\mathcal{A}_{\text{flat}})\dot{\theta}^-$ if $a_{\text{flat}} = 0$,
3. $\mathcal{M}\ddot{\theta} + \mathcal{N} + \mathcal{A}_{\text{flat}}^T \lambda = \tau_{\text{e}} + \tau_{\text{h}}$ if $|c_{\text{p}}(\theta, \dot{\theta})| < l_{\text{f}}$,
4. $\dot{\theta}^+ = \dot{\theta}^-, (\theta(1)^+, \theta(2)^+)^T = \mathcal{R}$ if $|c_{\text{p}}(\theta, \dot{\theta})| = l_{\text{f}}$,
5. $\mathcal{M}\ddot{\theta} + \mathcal{N} + \mathcal{A}_{\text{toe}}^T \lambda = \tau_{\text{e}} + \tau_{\text{h}}$ if $\mathcal{H}(\theta) \neq 0$,
6. $(\theta^+, \dot{\theta}^+) = \mathcal{D}(\theta^-, \dot{\theta}^-)$ if $\mathcal{H}(\theta) = 0$,

where $\mathcal{M} \in \mathbb{R}^{8\times 8}$ is the inertia matrix of the full biped model, and $\mathcal{N} \in \mathbb{R}^8$ groups the model's Coriolis and gravitational forces. The definitions for other dynamic terms can be found in [10]. Note that the vector $c_{\text{p}}(\theta, \dot{\theta})$ is the COM position defined with respect to the heel IRF and is used as a flag to detect contact conditions in simulation.

The overall torque input consists of both the human input vector $\tau_{\text{h}} \in \mathbb{R}^8$ and the exoskeleton input vector $\tau_{\text{e}} \in \mathbb{R}^8$. We assume the human input takes the form of a set-point PD controller that generates a stable limit cycle while walking down a shallow slope:

$$\tau_{\text{h}}^T = [0_{1\times 3}, \quad -(\theta_{\text{i}} - \bar{\theta}_{\text{i}})^T K_{\text{pi}}^T - \dot{\theta}_{\text{i}}^T K_{\text{di}}^T]^T,$$

where K_{pi}, K_{di}, θ_{i}, and $\bar{\theta}_{\text{i}}$ are constant values corresponding to the stiffness, viscosity, actual angle, and equilibrium angle of each joint, respectively. This form of human input is merely an assumption we make to simulate human walking, which does not represent real human neuromuscular input.

Due to the difficulty of analytically proving stability for hybrid systems in general, we checked local stability numerically by applying the Poincaré method. Letting $x = (\theta^T, \dot{\theta}^T)^T$ be the state vector of the full biped, a walking gait corresponds to a periodic solution curve $\bar{x}(t)$ of the hybrid system such that $\bar{x}(t) = \bar{x}(t + T)$, for all $t \geq 0$ and some minimal $T > 0$. The set of states occupied by the periodic solution defines a periodic orbit $\mathcal{O} := \{x | x = \bar{x}(t) \text{ for some } t\}$ in the state space. The step-to-step evolution of a solution curve can be modeled with the Poincaré map $\mathcal{P} : \mathcal{S} \to \mathcal{S}$, where $\mathcal{S} = \{x | \mathcal{H}(\theta) = 0\}$ is the switching surface indicating initial heel contact [26]. The intersection of a periodic orbit with the switching surface is a fixed point $x^* = \mathcal{P}(x^*)$. We can linearize the Poincaré map about this point to analyze the local stability of the hybrid dynamical system according to the standard result in [27]. If the eigenvalues of the Jacobian $\nabla_x \mathcal{P}(x^*)$ are within the unit circle, where $x^* = \mathcal{S} \cap \mathcal{O}$, then the periodic orbit $\mathcal{O}$ is locally exponentially stable in the hybrid system. The eigenvalues are calculated in simulation by first allowing the biped to converge to a fixed point and then by performing the perturbation analysis [28].

B. Energy Shaping Strategies

In our prior work, we chose to compensate for lower-limb inertia in the actuated part of a mass matrix, leaving the mass terms unshaped. In this section, we propose energy shaping strategies to shape all inertial terms in $\tilde{\mathcal{M}}_4$.

1) Defining $\tilde{\mathcal{M}}_4$: An interesting fact about the inertia matrix is the "cyclic-like" property on where the mass and inertia terms show up [9]. While traversing from the top-left corner to the bottom-right corner of the mass matrix, the number of links whose parameters appear in the matrix gradually decreases, indicating that each "layer" of the matrix carries a different weight in the overall kinetic energy. We respect this inherent property of the inertia matrix and choose the definition as

$$\tilde{\mathcal{M}}_4 = \begin{bmatrix} k_1\mathcal{M}_{(4,4)} & k_1\mathcal{M}_{(4,5)} & \dots & k_1\mathcal{M}_{(4,8)} \\ k_1\mathcal{M}_{(5,4)} & k_2\mathcal{M}_{(5,5)} & \dots & k_2\mathcal{M}_{(5,8)} \\ \vdots & \vdots & \ddots & \vdots \\ k_1\mathcal{M}_{(8,4)} & k_2\mathcal{M}_{(8,5)} & \dots & k_5\mathcal{M}_{(8,8)} \end{bmatrix}, \quad (12)$$

where $\mathcal{K}_1 = [k_1, k_2, \dots, k_5] \in \mathbb{R}^5$ is the parameter set to be determined and optimized. During simulation, we found out that for $\tilde{\mathcal{M}}$ being positive definite, k_1 and k_2 have to equal one. Therefore, the optimization problem reduces to finding the parameter set $\mathcal{K}_1 = [k_3, k_4, k_5] \in \mathbb{R}^3$.

As an alternative, we define $\tilde{M}_\lambda$ by scaling only the diagonal terms in $\mathcal{M}_4$ by $\mathcal{K}_2 = [k_\pi, k_\theta, k_\gamma] \in \mathbb{R}^3$, i.e.,

$$\tilde{\mathcal{M}}_4 = \begin{bmatrix} \dots & \dots & \dots & \dots \\ \dots & k_\pi\mathcal{M}_{(6,6)} & \mathcal{M}_{(6,7)} & \mathcal{M}_{(6,8)} \\ \dots & \mathcal{M}_{(7,6)} & k_\theta\mathcal{M}_{(7,7)} & \mathcal{M}_{(7,8)} \\ \dots & \mathcal{M}_{(8,6)} & \mathcal{M}_{(8,7)} & k_\gamma\mathcal{M}_{(8,8)} \end{bmatrix}. \quad (13)$$

2) Defining $\tilde{\mathcal{N}}$: Our prior definition of $\tilde{\mathcal{N}}$ in [29] scales all the shapeable rows by the same BWS ratio μ. However, this definition is only valid during fully-actuated contact conditions, e.g., the flat-foot condition. During heel and toe contact conditions, we cannot retrieve a valid closed-loop potential energy from this definition. Therefore, we adopt the definition presented in [30], i.e., only shape gravitational forces of each link that are perpendicular to the stance foot, to define $\tilde{\mathcal{N}}$ so that a valid potential energy can be retrieved across the entire gait cycle. These two strategies for potential energy can be represented as

$$\mu_s = \bar{\mu} \cdot I_{1\times 5} \in \mathbb{R}^5, \quad \mu_d = [\mu_1, \mu_2, \dots, \mu_5] \in \mathbb{R}^5,$$

where μ_s indicates using the same scaling factor $\bar{\mu}$ and μ_d indicates having a different μ_i for each row of $\mathcal{N}$, respectively. Having parameters $\bar{\mu} = 1$ or $\mu_i = 1$ implies not shaping the potential energy, i.e., $\tilde{\mathcal{N}} = \mathcal{N}$. More details regarding these definitions can be found in [30].

C. Results and Discussion

During simulation, we first tuned human joint impedance by trial and error to find a stable nominal gait. We then applied CMA-ES and BO to generate new populations of control parameters given some initial conditions. For both optimization algorithms, we simulated walking for 10 steps to

allow the gait to converge before computing the corresponding metrics. Once the gait converges, we applied the Poincaré section method to check the stability of the hybrid period orbit after each generation for CMA-ES, while for BO this stability was checked after each iteration. This corresponds to the "stability guaranteed" in Algorithms 1 and 2.

We chose different values for parameters in the sets $\mathcal{K}_1$, $\mathcal{K}_2$, μ_s, and μ_d to conduct simulation, where all eight different cases were chosen as shown in Table II. Note that strategy 1 includes the best hand-tuned parameters we found that yielded the most human torque reduction.

To ensure credible performance, we ran both the CMA-ES and BO six trials for each case in Table II. For safety reasons, we set the saturation for exoskeleton torque to be 50 Nm, and confined the values of $\bar{\mu}$ and $\mu_i, i \in \{1, \ldots, 5\}$ to be within $[0.4, 1.6]$ and k_i to be within $[0.75, 1.25]$, respectively. As opposed to the previous definitions in [10] which confined shaping variables to be less than one for providing assistance, we relaxed this condition in this paper, as adding virtual weight could possibly help humans swing their legs forward during late swing phase [31].

TABLE II
ENERGY SHAPING STRATEGIES FOR OPTIMIZATION

Strategy Number	Control Parameters $\mathbf{X}$
1	$k_3 = 0.9$, $k_4 = 0.8$, $k_5 = 0.5$, $\bar{\mu} = 0.9$
2	Only k_4 of $\mathcal{K}_1$, μ_s
3	$\mathcal{K}_1$, μ_s
4	μ_d
5	$\mathcal{K}_1$, μ_d
6	Different $\mathcal{K}_1$, μ_d for each contact phase
7	$\mathcal{K}_2$, μ_s
8	$\mathcal{K}_2$, μ_d

1) Human Torque Reduction: We show torque reduction (11) with different strategies in Fig. 2. Each bar represents the average of calculated metabolic cost over six trials. In general, CMA-ES and BO output similar results for each strategy. Based on the ascending trend from strategy 2 to 3, we can conclude that shaping more limb mass and inertia in $\tilde{\mathcal{M}}_4$ leads to more torque reduction. The similarity between strategies 4 and 5 shows that potential energy shaping is more dominant in deciding the overall reduction compared to kinetic energy shaping. The ascending trends from strategy 3 to 5 as well as strategy 7 to 8 indicate that having different potential energy shaping parameters are more helpful. Comparing strategies 3 and 7, as well as strategies 5 and 8, we can see that shaping the diagonal elements in $\tilde{\mathcal{M}}_4$ plays a more significant role than shaping the off-diagonal terms, i.e., the effect of shaping non-diagonal terms is almost negligible.

Finally, strategy 6 adopts three different sets of ($\mathcal{K}_1$, μ_d) for each contact condition, and this strategy outmatches the other cases in terms of reduction percentage. The optimal parameters of this strategy are given in Table III, where each cell includes both the parameters from CMA-ES and BO (before and after "/", respectively). We can see that some of the parameters are greater than one, which verifies our assumption that adding virtual weight and inertia can

TABLE III
OPTIMAL CONTROL PARAMETERS OF STRATEGY 6

CMA-ES/BO	Heel Contact	Flat Foot	Toe Contact
k_3	1.009/1.072	0.931/0.862	0.958/1.011
k_4	1.096/1.098	1.051/0.894	1.075/0.981
k_5	1.005/1.101	0.924/0.918	0.984/1.038
μ_1	0.936/1.022	0.993/1.088	0.994/1.090
μ_2	1.084/0.743	1.056/1.146	1.025/0.868
μ_3	1.078/1.108	0.763/0.874	0.993/1.011
μ_4	1.094/0.834	0.729/0.570	1.139/1.152
μ_5	1.029/0.743	0.584/0.530	1.101/1.140

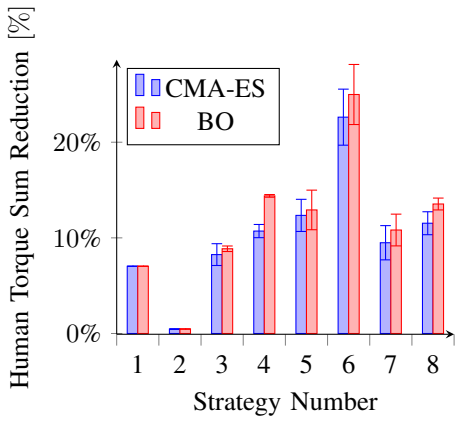

Fig. 2. The human torque sum reduction (compared to the passive gait) for different strategies using CMA-ES and BO with ± 1 standard deviation.

be actually helpful in providing assistance. We also tried to simulate walking using different sets of $\mathcal{K}_1$ and μ_s for each contact condition. However, positive definiteness of $\tilde{\mathcal{M}}_\lambda$ cannot be ensured.

2) Metabolic Cost Reduction: To further study the benefits of the proposed framework, we adopted the following metric

$$E_{\text{walking}} = (E_{\text{3LP}} + E_{\text{CR}} + E_{\text{GC}})/\eta + E_{\text{WS}}, \tag{14}$$

$$E_{\text{3LP}} = \int_0^T [\frac{\mathrm{d}}{\mathrm{dt}}(\frac{1}{2}\dot{q}^T\tilde{\mathcal{M}}\dot{q})]^+ \mathrm{dt},$$

$$E_{\text{CR}} = \frac{1}{2}\tilde{\mathcal{M}}v_z^2, \quad E_{\text{GC}} = 2m_{\text{leg}}\mathcal{H}(\theta)g,$$

$$E_{\text{WS}} = \int_0^T m_{\text{leg}}g\cos(\beta)l_t \sin(\frac{\theta_{\text{k}}}{2})\dot{\theta}_{\text{kmax}}\Phi(\frac{\dot{\theta}_{\text{k}}}{\dot{\theta}_{\text{kmax}}})\mathrm{dt},$$

proposed in [32] to compute the metabolic cost of simulated walking with each strategy. The first term E_{3LP} in (14) represents the swing and torso balance cost of the 3-link linear pendulum model, the second term E_{CR} denotes the energy cost to compensate for the COM vertical velocity change due to impacts. The third term E_{GC} denotes the cost of maintaining proper ground clearance, and the last term E_{WS} indicates the weight support cost. Among these definitions, m_{leg} is the overall mass of the leg, v_z is the vertical COM velocity, β is the stance leg angle with respect to gravity, l_t is the thigh length, $\eta = 0.25$ is the assumed muscle efficiency, and $\Phi(\cdot)$ is the Alexander-Minetti's cost curve [32].

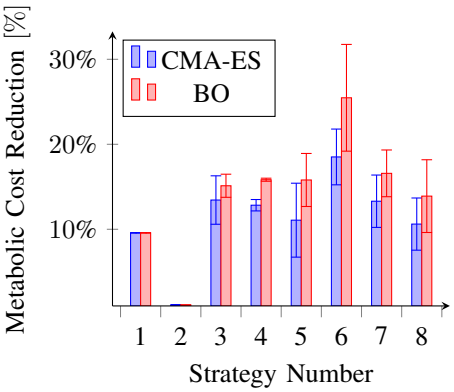

Fig. 3. The mean and ± 1 standard deviation of E_{walking} calculated based on different strategies with optimal parameters. The zero line in y-axis indicates the metabolic cost of passive gait.

Similar to Fig. 2, we computed the mean value and the standard deviation of E_{walking} across six trials for each strategy and compare them with the cost of the passive gait. From Fig. 3, we can see that all strategies are able to reduce metabolic costs, among which strategy 6 yields the most reduction. These data not only comply with the conclusion we draw from Fig. 2 but also indicate the proposed strategies can effectively reduce metabolic cost during simulated walking.

3) Normative Kinematic Data: To demonstrate the proposed framework is capable of providing task-variant assistance across subjects and tasks, we compute exoskeleton torque (10) using able-bodied human subjects' normative kinematic data [33] with parameters from Table III. Fig. 4 compares estimated exoskeleton joint torques for the decline, level and incline conditions, respectively.

The main phases during stance that require exoskeleton assistance are weight absorption and push-off [34]. To assist able-bodied persons, knee extension and ankle plantar flexion torque should be provided via exoskeleton at terminal stance to swing the limbs upwards. From Fig. 4, we can see exoskeleton torques with optimal parameters closely match the real human torques, especially at the ankle joint. Compared to the aggressive ankle torque at terminal stance in [10], the optimal strategies in this paper provide mild assistance, which is critical in assisting human locomotion [31]. In addition, the optimal shaping strategies provide necessary knee extension torques in weight absorption as well as in late stance to propel the body forward for all three conditions. This again is an improvement compared to the potential energy shaping strategy proposed in [12], which provides flexion torques during level and incline conditions that are counterproductive. With our prior experimental results on energy shaping across various activities [10] and the results presented in Fig. 4, we can safely assume the proposed task-invariant framework is capable of finding optimal parameters across subjects and daily activities such as stair ascent and descent.

Conclusion and Future Work

In this paper, we present a task-invariant learning framework for lower-limb exoskeletons to minimize human joint torques and metabolic cost across locomotor tasks. Built upon our prior framework on underactuated energy shaping, we incorporate derivative-free, sample efficient optimization algorithms, i.e., CMA-ES and BO, to automatically update the parameters of task-invariant energy shaping strategies through online iteration. Simulation results on a human-like biped demonstrated that all the optimized strategies can effectively reduce human joint torque and estimated metabolic cost. Among these strategies, the optimal exoskeleton torques calculated using able-bodied subjects' kinematics closely match real human joint torques. These torques also provide milder assistance during weight absorption and terminal stance, which is an improvement compared to our prior results on potential energy shaping. Future work includes experimental implementation on physical exoskeletons and refining the framework to automatically search for assistive strategies.

References

[1] G. Zeilig, H. Weingarden, M. Zwecker, I. Dudkiewicz, A. Bloch, and A. Esquenazi, "Safety and tolerance of the ReWalk$^{\text{TM}}$ exoskeleton suit for ambulation by people with complete spinal cord injury: A pilot study," *The Journal of Spinal Cord Medicine*, vol. 35, no. 2, pp. 96–101, 2012.

[2] S. A. Kolakowsky-Hayner, J. Crew, S. Moran, and A. Shah, "Safety and feasibility of using the Ekso$^{\text{TM}}$ Bionic exoskeleton to aid ambulation after spinal cord injury," *J Spine*, vol. 4, p. 003, 2013.

[3] D. Sanz Merodio, M. Cestari Soto, J. C. Arevalo, and E. García Armada, "Control motion approach of a lower limb orthosis to reduce energy consumption," *Int. J. Adv. Robot. Syst.*, vol. 9, pp. 1–8, 2012.

[4] R. Ferris, H. Quintero, and M. Goldfarb, "Preliminary evaluation of a powered lower limb orthosis to aid walking in paraplegic individuals," *IEEE Trans. Neural Syst. Rehabil. Eng.*, vol. 19, no. 6, pp. 652–659, 2011.

[5] T. Yan, M. Cempini, C. M. Oddo, and N. Vitiello, "Review of assistive strategies in powered lower-limb orthoses and exoskeletons," *Rob. Auton. Syst*, vol. 64, pp. 120–136, 2015.

[6] R. Jimenez-Fabian and O. Verlinden, "Review of control algorithms for robotic ankle systems in lower-limb orthoses, prostheses, and exoskeletons," *Medical Engineering & Physics*, vol. 34, no. 4, pp. 397–408, 2012.

[7] M. W. Spong, "The passivity paradigm in bipedal locomotion," in *Proceedings of the International Conference on Climbing and Walking Robots*, Madrid, Spain, 2004.

[8] M. W. Spong, J. K. Holm, and D. Lee, "Passivity-based control of bipedal locomotion," *IEEE Rob. Autom. Mag.*, vol. 14, no. 2, pp. 30–40, 2007.

[9] R. D. Gregg and M. W. Spong, "Reduction-based control of three-dimensional bipedal walking robots," *Int. J. Rob. Res.*, vol. 29, no. 6, pp. 680–702, 2010.

[10] G. Lv, H. Zhu, and R. D. Gregg, "On the design and control of highly backdrivable lower-limb exoskeletons: A discussion of past and ongoing work," *IEEE Control Syst. Mag.*, vol. 38, no. 6, pp. 88–113, 2018.

[11] G. Lv and R. Gregg, "Towards total energy shaping control of lower-limb exoskeletons," in *American Control Conference (ACC), 2017*. IEEE, 2017, pp. 4851–4857.

[12] G. Lv and R. D. Gregg, "Underactuated potential energy shaping with contact constraints: Application to a powered knee-ankle orthosis," *IEEE Trans. Control Syst. Technol.*, vol. 26, no. 1, pp. 181–193, 2018.

[13] G. Lv, H. Zhu, T. Elery, L. Li, and R. D. Gregg, "Experimental implementation of underactuated potential energy shaping on a powered ankle-foot orthosis," in *IEEE Int. Conf. Robot. Autom.*, 2016, pp. 3493–3500.

[14] M. Franceschini *et al.*, "Walking after stroke: What does treadmill training with body weight support add to overground gait training in patients early after stroke? A single-blind, randomized, controlled trial," *Stroke*, vol. 40, no. 9, pp. 3079–3085, 2009.

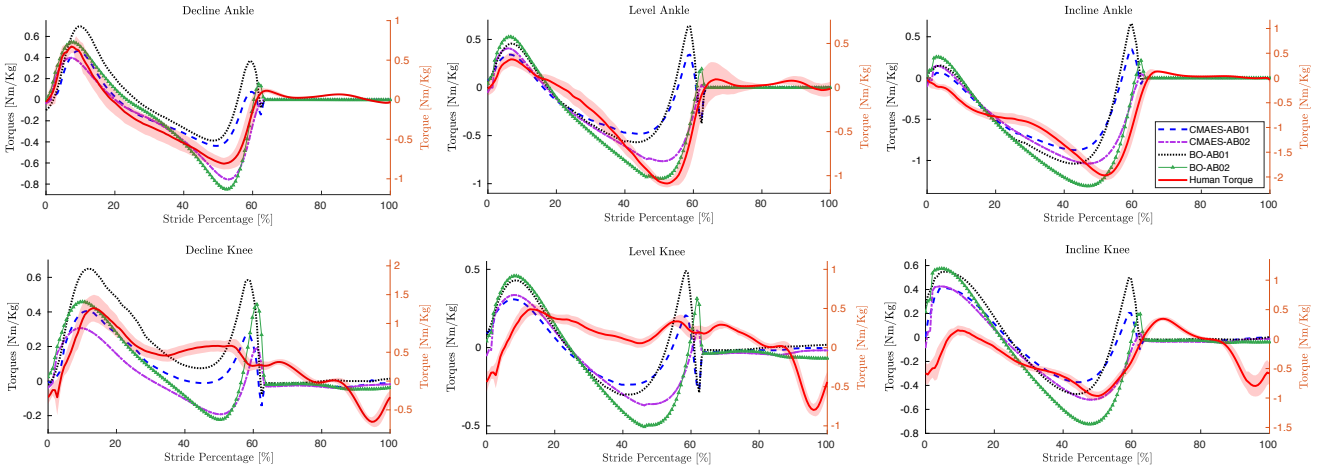

Fig. 4. Exoskeleton torques calculated using parameters from Table III and kinematic data of two able-bodied subjects from [33] . From left to right: the torques acting on ankles and knees based on decline ($-10°/-7.5°$), level ground ($0°$), and incline ($10°/7.5°$) walking on a treadmill with velocity equaling 1.2 m/s and 0.8 m/s. The number before and after "/ " indicates the test conditions for subject 1 and subject 2, respectively. The red solid lines represent the averaged human torques with variance. Positive values represent ankle dorsiflexion torques and knee extension torques.

[15] S. H. Collins, M. B. Wiggin, and G. S. Sawicki, "Reducing the energy cost of human walking using an unpowered exoskeleton," *Nature*, vol. 522, no. 7555, pp. 212–215, 2015.

[16] J. Zhang, P. Fiers, K. A. Witte, R. W. Jackson, K. L. Poggensee, C. G. Atkeson, and S. H. Collins, "Human-in-the-loop optimization of exoskeleton assistance during walking," *Science*, vol. 356, no. 6344, pp. 1280–1284, 2017.

[17] Y. Ding, M. Kim, S. Kuindersma, and C. J. Walsh, "Human-in-the-loop optimization of hip assistance with a soft exosuit during walking," *Science Robotics*, vol. 3, no. 15, p. eaar5438, 2018.

[18] N. Hansen, S. D. Müller, and P. Koumoutsakos, "Reducing the time complexity of the derandomized evolution strategy with covariance matrix adaptation (cma-es)," *Evolutionary computation*, vol. 11, no. 1, pp. 1–18, 2003.

[19] M. Pelikan, D. E. Goldberg, and E. Cantú-Paz, "Boa: The bayesian optimization algorithm," in *Proceedings of the 1st Annual Conference on Genetic and Evolutionary Computation-Volume 1*. Morgan Kaufmann Publishers Inc., 1999, pp. 525–532.

[20] A. Rai, R. Antonova, F. Meier, and C. G. Atkeson, "Using simulation to improve sample-efficiency of bayesian optimization for bipedal robots." *Journal of machine learning research*, vol. 20, no. 49, pp. 1–24, 2019.

[21] A. Martin and J. Schmiedeler, "Predicting human walking gaits with a simple planar model," *J. Biomech.*, vol. 47, no. 6, pp. 1416–1421, 2014.

[22] A. Silder, T. Besier, and S. L. Delp, "Predicting the metabolic cost of incline walking from muscle activity and walking mechanics," *J. Biomech.*, vol. 45, no. 10, pp. 1842–1849, 2012.

[23] R. M. Murray, Z. Li, and S. S. Sastry, *A Mathematical Introduction to Robotic Manipulation*. CRC press, 1994.

[24] M. Kim, Y. Ding, P. Malcolm, J. Speeckaert, C. J. Siviy, C. J. Walsh, and S. Kuindersma, "Human-in-the-loop bayesian optimization of wearable device parameters," *PloS one*, vol. 12, no. 9, p. e0184054, 2017.

[25] P. I. Frazier, "A tutorial on bayesian optimization," *arXiv preprint arXiv:1807.02811*, 2018.

[26] R. D. Gregg, T. Lenzi, L. J. Hargrove, and J. W. Sensinger, "Virtual constraint control of a powered prosthetic leg: From simulation to experiments with transfemoral amputees," *IEEE Trans. Rob.*, vol. 30, no. 6, pp. 1455–1471, 2014.

[27] J. Grizzle, E. Westervelt, C. Chevallereau, J. Choi, and B. Morris, *Feedback Control of Dynamic Bipedal Robot Locomotion*. Boca Raton, FL: CRC Press, 2007.

[28] R. D. Gregg, Y. Y. Dhaher, A. Degani, and K. M. Lynch, "On the mechanics of functional asymmetry in bipedal walking," *IEEE Trans. Biomed. Eng*, vol. 59, no. 5, pp. 1310–1318, 2012.

[29] J. Lin, G. Lv, and R. D. Gregg, "Contact-invariant total energy shaping control for powered exoskeletons," in *2019 American Control Conference (ACC)*. IEEE, 2019, pp. 664–670.

[30] J. Lin, N. Divekar, G. Lv, and R. D. Gregg, "Energy shaping control with virtual spring and damper for powered exoskeletons," in *Prof. IEEE Conf. Decis. Control*. IEEE, 2019, pp. 3039–3045.

[31] D. A. Winter, *Biomechanics and Motor Control of Human Movement*. John Wiley & Sons, 2009.

[32] S. Faraji, A. R. Wu, and A. J. Ijspeert, "A simple model of mechanical effects to estimate metabolic cost of human walking," *Scientific reports*, vol. 8, no. 1, p. 10998, 2018.

[33] K. R. Embry, D. J. Villarreal, R. L. Macaluso, and R. D. Gregg, "Modeling the kinematics of human locomotion over continuously varying speeds and inclines," *IEEE Trans. Neural Syst. Rehabil. Eng.*, vol. 26, no. 12, pp. 2342–2350, 2018.

[34] J. Boudarham, R. Zory, F. Genet, G. Vigné, D. Bensmail, N. Roche, and D. Pradon, "Effects of a knee–ankle–foot orthosis on gait biomechanical characteristics of paretic and non-paretic limbs in hemiplegic patients with genu recurvatum," *Clinical Biomechanics*, vol. 28, no. 1, pp. 73–78, 2013.